JOURNAL OF MATERIALS SCIENCE 29 (1994) 3085–3094

Critical splitting of the solidifying interface–geometrical model of spacing selection during directional solidification of lamellar eutectics

JUN-MING LIU, ZHI-GUO LIU, ZHUANG-CHUN WU
National Laboratory of Solid State Microstructures, Nanjing University, Nanjing 210008, People's Republic of China

The steady-state coupling equations of directional solidification of Al–Al_2Cu ($\varepsilon = 0.94$), Sn–Pb ($\varepsilon = 0.59$)and Al–Si ($\varepsilon = 0.17$)eutectics have been solved numerically. The profiles, splitting features and supercooling of the solidifying interface were investigated in detail as functions of the lamellar spacing. It was found that when supercooling, ΔT_0, at the three-phase conjunction point reaches its minimum value, min (ΔT_0), the solidifying interface profile of one lamellar phase was in the critical splitting state (marginally stable state) and that of the other lamella was super-stable. Langer's marginal stability theory of lamellar eutectic solidification with a planar interface was extended to the case with a curved interface, and a geometrical model of the spacing selection has been suggested (critical splitting state of one lamella's solidifying interface). The general scaling law of the spacing, derived according to this theory, was found to be consistent with the similarity law recently derived by Kassner and Misbah; it is also supported by experimental results. Another geometrical model of the spacing selection was found, where the solidifying interface profile of one lamella became split and other lamella's profile was in the critical splitting state. The experimental data for directional solidification of Al–Si eutectic showed that the irregular eutectics have a spacing selected according to this mode.

1. Introduction

When a eutectic is submitted to directional solidification, the solidifying interface forms parallel lamellae of two coexisting solid phases, α and β. This problem is of interest both from the view point of technological applications [1, 2] and, more fundamentally, as an example of spontaneous pattern formation in nature. In the last decades, many physicists and metallurgists have made much effort to predict the spacing selection of lamellar eutectic [3]. It is well known that supercooling, ΔT, of the solidifying interface and the lamellar spacing, λ, are uniquely determined by the solidifying rate, V. Based on the assumption of a planar solidifying interface, the theoretical approach to this problem shows ΔT can be formulated as a function of V and λ [4]

$$\Delta T = K_1 \lambda V + K_2/\lambda \quad (1)$$

where K_1 and K_2 are, respectively, the constitutional supercooling effect and the Gibbs–Thompson effect of the solidifying interface. This relation allows wide selection ranges of both λ and ΔT for a given V, and therefore it cannot predict unique values of λ and ΔT, as shown by experiments. This problem is similar in form to the formation of a dendritic pattern in the growth of binary mixture [5] and evolution of viscous fingers in the Hele–Shaw cell [6], and hence belongs to a class of pattern-formation problems far from equilibrium in nature which are controlled by the Laplace field. Generally, a dynamic selection principle (precisely speaking, a dynamic conjecture) needs to be induced in order to solve this problem. For the present case, the minimum supercooling conjecture is commonly used [7] and the following scaling relation can be obtained from Equation 1 [4]

$$\lambda \simeq V^{-1/2} \quad (2)$$

This relation is strongly supported by many experimental results. Further, Langer and co-worker [8, 9] and Cline [10–14] verified that this conjecture coincides with the operating point of dynamically marginal stability. The problem seems to be solved.

Unfortunately, following deep discussion about this problem above, we suspect the generality of the scaling relation, Equation 2. At first, we notice that the profile of the solidifying interface must be curved. This is naturally determined by the coupling of constitutional supercooling and the Gibbs–Thompson effect (if we neglect the kinetic effect) of the solidifying interface. Secondly, in the case for a curved solidifying interface, is Langer's stability theory [8], based on the assumption of planar solidifying interface, valid? Even if we pre-assume its validity, precisely speaking, at this time, we do not know which point of the interface this

0022–2461

theory should be applied to, because only the supercooling, $\Delta T(x)$ at a point x of the curved interface, has any physical meaning. If V is high, the interface can be approached as a plane, because λ is much less than the thermal diffusion length. If V is low, this approach is invalid. To our knowledge, the cases with $V < 10\ \mu m\ s^{-1}$ have not been investigated experimentally to any great extent. Therefore, at least in the case where V is low, the validity of Equation 2 should be suspected. Finally, the profile of the solidifying interface forms self-consistently. Under conditions of directional solidification, the geometrical features of the interface in fact are determined by the coupling of the thermal transfer, the solute diffusion and also the Gibbs–Thompson effect, and hence can reflect the dynamic behaviour of spacing selection. The planar interface approximation arbitrarily discards this coupling and the non-linear characteristics of the spacing selection dynamics.

In this paper, attention is paid to the geometrical features of the solidifying interface and the dynamic behaviour of the spacing selection by solving numerically the non-linear steady-state coupling equation of directional solidification of a lamellar eutectic. It will be proved that the critical splitting state (CSS) of the solidifying interface of, at least, one lamellar phase, corresponds to the minimum supercooling at the three-phase conjunction point (TPCP); at this time, the solidifying interface forms in the stability limit (i.e. marginally stable). A new selection mechanism of the spacing – the critical splitting model of the solidifying interface – is suggested. The general scaling laws, derived according to this model, are consistent with the similarity law derived by Kassner and Misbah [15]. Finally, the selection problem of spacing of an irregular eutectic during directional solidification is also discussed.

2. Coupling equation and numerical calculation

In the coordinate system shown in Fig. 1, the profiles of α-liquid and β-liquid interfaces are expressed by $f(x)$ and $g(x)$, respectively. The coupling equation can be written as [16]

$$\Delta T_0 - Gf(x) = \sum_{n=1}^{\infty} m_\alpha K \cos\left(\frac{2n\pi}{\lambda}x\right) - \frac{\Gamma^\alpha f''(x)}{[1 + f'^2(x)]^{3/2}} \qquad 0 \le x \le S_\alpha \quad (3a)$$

$$\Delta T_0 - G\,g(x) = \sum_{n=1}^{\infty} -m_\beta K \cos\left(\frac{2n\pi}{\lambda}x\right) - \frac{\Gamma^\beta g''(x)}{[1 + g'^2(x)]^{3/2}} \qquad S_\alpha < x \le S_\alpha + S_\beta \quad (3b)$$

$$K = \left(\frac{V\lambda}{D}\right)\left(\frac{C_0}{n^2\pi^2}\right)\sin\left(\frac{2n\pi}{\lambda}S_\alpha\right) \quad (3c)$$

where m_α and m_β are the absolute values of the liquidus slopes of α and β phases, respectively, D is the solute diffusion coefficient, G is the temperature gradient in the liquid in front of the solidifying interface, Γ^α and Γ^β are the Gibbs–Thompson coefficients of the α-liquid and β-liquid interfaces, respectively, C_0 is the difference between the maximum solubilities of the two phases. ΔT_0 is the supercooling at the TPCP. For the detailed derivation of Equation 3, please refer to Liu *et al.* [16]. The boundary conditions are

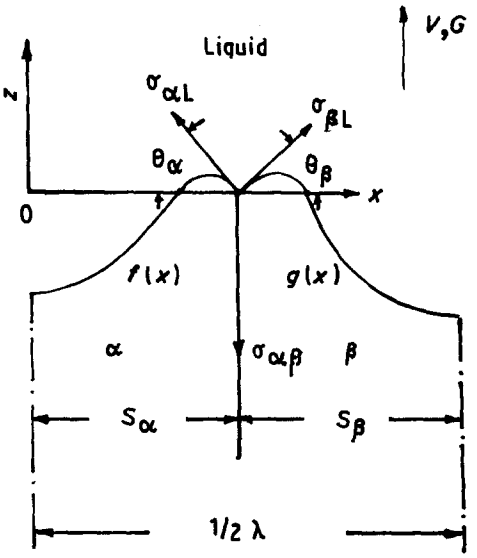

Figure 1 The coordinate system and profile of the solidifying interface of a lamellar eutectic. The spacing of the periodical interface is denoted by λ.

$$f(x) = g(x) = 0 \quad \text{as } x = S_\alpha \quad (4a)$$

$$f'(x) = -tg\theta_\alpha, g'(x) = tg\theta_\beta \quad \text{as } x = S_\alpha \quad (4b)$$

$$f'(x = 0) = 0,\ g'(x = S_\alpha + S_\beta = \lambda/2) = 0 \quad (4c)$$

where θ_α and θ_β are the groove angles of the α-liquid and β-liquid interfaces at the TPCP, which are determined by the mechanical balance condition at the TPCP.

As V and G are given, another boundary condition besides Equation 4 is required to obtain unique solutions of λ, ΔT_0, $f(x)$ and $g(x)$ from Equation 3. In Equation 3 the temperature gradient dependence of solidification is included, which is, in fact, proved to be considerable at low V by some experiments.

Equation 3 will be solved by the finite difference method. We have noticed that the ratio $\varepsilon (= S_\beta/S_\alpha)$ in volume of two lamellar phases as a key physical parameter has considerable influence on the profile of the solidifying interface. Therefore, Al(α)–Al_2Cu(β) ($\varepsilon = 0.935$), Sn(α)–Pb(β) ($\varepsilon = 0.594$), Al(α)–Si(β) ($\varepsilon = 0.167$) eutectics have been selected as the objects of our numerical calculations. The physical parameters of the three eutectics are listed in Table I [4, 17, 18], where values of θ_α and θ_β are calculated from the mechanical balance condition

$$\sigma_{\alpha L}\cos\theta_\alpha = \sigma_{\beta L}\cos\theta_\beta \quad (5a)$$

$$\sigma_{\alpha L}\sin\theta_\alpha + \sigma_{\beta L}\sin\theta_\beta = \sigma_{\alpha\beta} \quad (5b)$$

Of the three eutectics, the case of Al–Si is the most complicated. For this eutectic, ΔT_0 terms in Equa-

TABLE I Some physical parameters of Al–Al_2Cu, Sn–Pb, Al–Si eutectics [4, 17, 18]

	m_α (K/wt%)	m_β (K/wt%)	Γ^α (K μm)	Γ^β (K μm)	$C_{\alpha m}$ (wt%)	$C_{\beta m}$ (wt%)	C_0 (wt%)	C_E (wt%)	D ($\mu m^2 s^{-1}$)	ε	θ_α (deg)	θ_β (deg)	$\sigma_{\alpha L}$ (erg cm^{-2})	$\sigma_{\beta L}$ (erg cm^{-2})	$\sigma_{\alpha\beta}$ (erg cm^{-2})
Al–Al_2Cu	4.6	4.8	0.241	0.245	5.65	52.50	46.83	33.20	3260	0.9353	30	26	140	133	124
Sn–Pb	1.2	3.5	0.0785	0.0475	≃ 10	≃ 79.55	69.55	26.10	717	0.5940	56.5	10	132.43	74	123
Al–Si	8.3	20	0.196	0.170	1.65	100.00	98.35	12.62	5000	0.1669	30	65.5	169.0	352	404.8

tion 3a and b are not equivalent to each other, which are respectively denoted by ΔT_0^α and ΔT_0^β. We find the ratio $\Delta T_0^\alpha / \Delta T_0^\beta \cong \varepsilon$. This is a large defect for our model. In fact, at the TPCP ($x = S_\alpha$, $z = 0$), strong co-diffusion must occur between α and β phases, and in addition, the local equilibrium condition of thermodynamics will be invalid within a small range around this point. We are convinced that $\Delta T_0^\alpha \equiv \Delta T_0^\beta$, under directional solidification conditions. Here, we still proceed by considering the validity of the local equilibrium condition, and hence treat ΔT_0^α and ΔT_0^β as two physical parameters for the case of Al–Si eutectic.

In the numerical calculations, attention is given to the profile, the splitting features and the supercooling terms of the solidifying interface. The detailed procedures of the calculation are omitted owing to their simplicity.

3. Results and discussion

3.1. Interfacial supercooling

As pointed out above, only supercooling at a point of the solidifying interface has any physical meaning. Here, we discuss the supercooling at the TPCP, ΔT_0, and the average supercooling, $\overline{\Delta T}$. (For Al–Si eutectic, correspondingly, ΔT_0^α and ΔT_0^β, $\overline{\Delta T_\alpha}$ and $\overline{\Delta T_\beta}$). The definitions of these average supercooling terms are as follows

$$\overline{\Delta T} = \Delta T_0 - \frac{G}{1+\varepsilon}[\overline{f(x)} + \varepsilon \overline{g(x)}] \quad (6a)$$

$$\overline{\Delta T_\alpha} = \Delta T_0^\alpha - G\overline{f(x)} \quad (6b)$$

$$\overline{\Delta T_\beta} = \Delta T_0^\beta - G\overline{g(x)} \quad (6c)$$

$$\overline{f(x)} = \frac{1}{S_\alpha}\int_0^{S_\alpha} f(x)\,dx,$$

$$\overline{g(x)} = \frac{1}{S_\beta}\int_{S_\alpha}^{S_\alpha + S_\beta} g(x)\,dx \quad (6d)$$

As functions of the spacing λ, ΔT_0 ($\Delta T_0^\alpha, \Delta T_0^\beta$), $\overline{\Delta T}$ ($\overline{\Delta T_\alpha}, \overline{\Delta T_\beta}$) are calculated, respectively, as shown in Figs 2–4. In general, the supercooling ΔT_0 ($\Delta T_0^\alpha, \Delta T_0^\beta$) can be expressed as

$$\Delta T_0 = a\lambda V + b/\lambda, \quad a > 0, \quad b > 0 \quad (7)$$

Thus, as a function of λ, ΔT_0 ($\Delta T_0^\alpha, \Delta T_0^\beta$) has a minimum value, $\min(\Delta T_0)$, and the spacing-dependent upper curve of ΔT_0 behaves in a concave manner. $\overline{\Delta T}$ ($\overline{\Delta T_\alpha}, \overline{\Delta T_\beta}$) has the similar form to Equation 7 and has also a minimum value, $\min(\overline{\Delta T})$. Interestingly, at high V, the difference between ΔT_0 (ΔT_0^β) and $\overline{\Delta T}$ ($\overline{\Delta T_\beta}$) is small, and the minimum value positions of ΔT_0 (ΔT_0^β) and $\overline{\Delta T}$ ($\overline{\Delta T_\beta}$) as functions of λ, denoted, respectively, by λ_1 and λ_2, (i.e. $\lambda_1 = \lambda|_{\Delta T_0 = \min(\Delta T_0)}$ and $\lambda_2 = \lambda|_{\overline{\Delta T} = \min(\overline{\Delta T})}$), are consistent with each other; however, at low V, large difference between ΔT_0 and $\overline{\Delta T}$ appears, and λ_1 moves considerably towards the left from λ_2. If we now apply Langer's marginal stability theory [8, 9] to determine the spacing, λ, forming during solidification, we may have two mechanisms to be selected: λ_1 and λ_2.

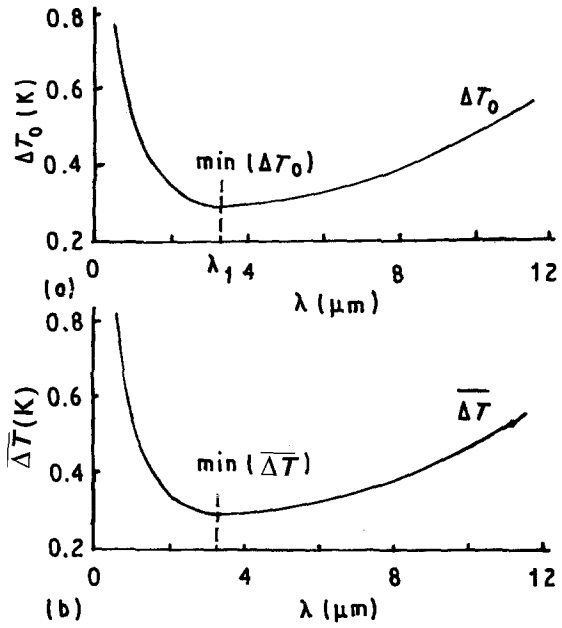

Figure 2 (a) Supercooling, ΔT_0, at the TPCP and (b) the average supercooling, $\overline{\Delta T}$, as functions of the lamellar spacing, λ, for directional solidification of Al–Al_2Cu eutectic. $V = 10\ \mu m\,s^{-1}$, $G = 110\ K\,cm^{-1}$, $\lambda_1 = 3.30\ \mu m$, $\lambda_2 = 3.33\ \mu m$.

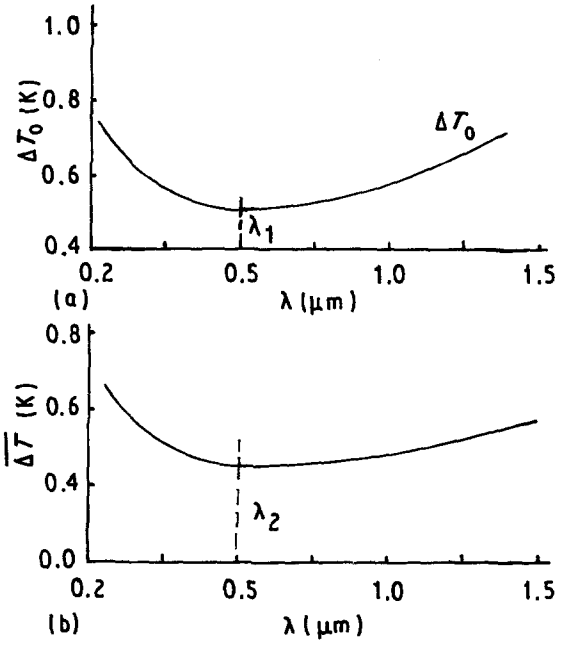

Figure 3 (a) Supercooling, ΔT_0, at the TPCP and (b) the average supercooling, $\overline{\Delta T}$, as functions of the lamellar spacing, λ, for directional solidification of Sn–Pb eutectic. $V = 30\ \mu m\,s^{-1}$, $G = 100\ K\,cm^{-1}$, $\lambda_1 = 0.50\ \mu m$, $\lambda_2 = 0.51\ \mu m$.

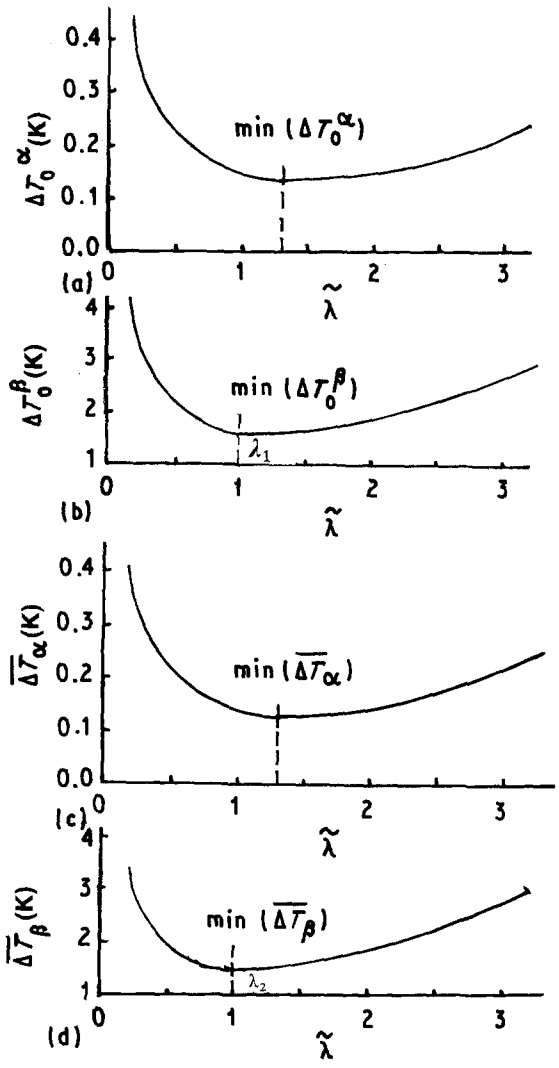

Figure 4 Supercooling terms, (a) ΔT_0^{α} and (b) ΔT_0^{β}, at the TPCP and the average supercooling terms, (c) $\overline{\Delta T}_{\alpha}$ and (d) $\overline{\Delta T}_{\beta}$, as functions of the lamellar spacing, λ, for directional solidification of Al–Si eutectic. $V = 10\ \mu m\,s^{-1}$, $G = 110\ K\,cm^{-1}$, $\tilde{\lambda} = \lambda/\lambda_1$, $\lambda_1 = 2.70\ \mu m$, $\lambda_2 = 2.71\ \mu m$.

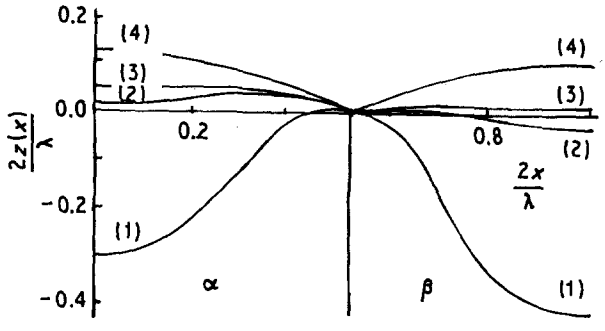

Figure 5 Profiles of the solidifying interface with different spacings, λ, for directional solidification of Al–Al_2Cu eutectic. $V = 2.00\ \mu m\,s^{-1}$; $G = 110\ K\,cm^{-1}$; (1) $\lambda \approx 30.0\ \mu m$; (2) $\lambda = 15.0\ \mu m$; (3) $\lambda = 12.00\ \mu m$; (4) $\lambda = 1.00\ \mu m$.

3.2. Interfacial profile

From Equation 3, we infer considerable dependence of the interfacial profile on the spacing as V and G are given. The planar approximation of the interfacial profile is obviously invalid. Figs 5–7 show calculated profiles of the solidifying interface with different spacings for the three eutectics. When the spacing λ increases, in the normalized coordinate systems shown in Fig. 5–7, the interfacial profile moves relative to the TPCP to the solid side. As λ is very small, the interfacial profile bulges into the liquid range; however, the middle part of the interfacial profile becomes considerably concave to the solid side, because λ is large. Obviously, for the latter case, the weak curvature effect of the interface indicates the domination of the constitutional supercooling in front

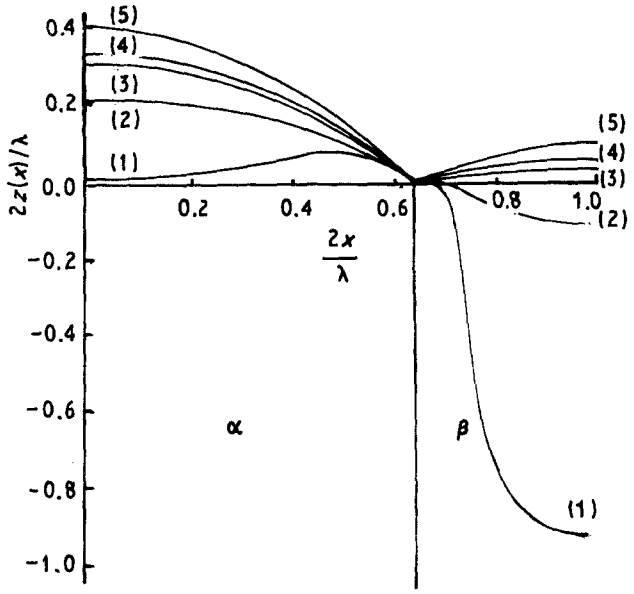

Figure 6 Profiles of the solidifying interface with different spacings, λ, for directional solidification of Sn–Pb eutectic. $V = 5.00\ \mu m\ s^{-1}$, $G = 100\ K\ cm^{-1}$; (1) $\lambda = 5.00\ \mu m$; (2) $\lambda = 3.00\ \mu m$; (3) $\lambda = 1.20\ \mu m$; (4) $\lambda = 0.10\ \mu m$; (5) $\lambda = 0.05\ \mu m$.

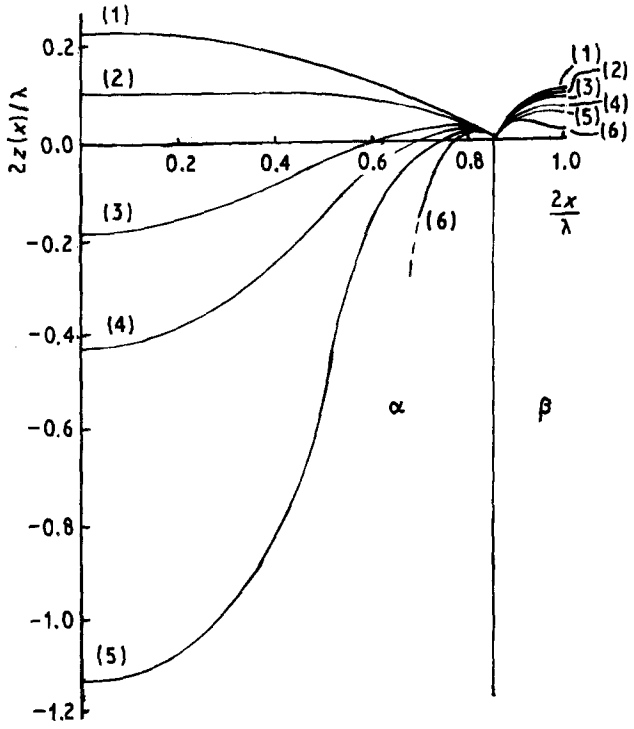

Figure 7 Profiles of the solidifying interface with different spacings, λ, for directional solidification of Al–Si eutectic. $V = 2.00\ \mu m\ s^{-1}$; $G = 110\ K\ cm^{-1}$; (1) $\lambda = 0.50\ \mu m$; (2) $\lambda = 2.70\ \mu m$; (3) $\lambda = 5.00\ \mu m$; (4) $\lambda = 7.00\ \mu m$; (6) $\lambda = 9.50\ \mu m$.

of the concave middle range of the interface, which will result in further movement of the interface to the solid side until a new lamellar phase forms in the concave liquid range. At this time, the local lamellar spacing will fall to half the initial spacing. Conversely, the curvature effect, the thermal transfer and the mechanical balance condition at the TPCP will restrain the tendency of movement to the liquid side of the bulging interfacial profile, because λ is very small. Therefore, a stable interfacial profile will bulge slightly into the liquid range; and the concave interfacial profile on the solid side will be unstable.

The temperature gradient dependence of the interfacial profile was also calculated. We found that the profile was compelled to recover to the planar state as G increased. However, this dependence only became considerable at low V.

3.3. Splitting the solidifying interface

From Figs 5–7, it is noticed that the interface profile splits when λ increases. For symmetry reasons, $f''(x = 0)$ and $g''(x = \lambda/2)$ can be used to characterize the splitting features of the interfacial profiles, $f(x)$ and $g(x)$, respectively. In the coordinate system shown in Fig. 1, the interfacial profile has split as $f''(x = 0) \geq 0$ ($g''(x = \lambda/2) \geq 0$); the profile bulges into the liquid side as $f''(x = 0) < 0$ ($g''(x = \lambda/2) < 0$). The latter case is termed the super-stable state.

A detailed investigation of the splitting features was made. $f''(x = 0)$ and $g''(x = \lambda/2)$ were calculated as functions of λ for the three eutectics. The results are shown in Figs 8–10; in Fig. 10 we use the normalized coordinate: $\tilde{\lambda} = \lambda/\lambda_1$. λ_1 is defined in Section 3.1. Interestingly, we find that for the three eutectics, $f''(x = 0)$ and/or $g''(x = \lambda/2) = 0$ as $\tilde{\lambda} = 1.0$. This indicates that when the supercooling ΔT_0 at the TPCP

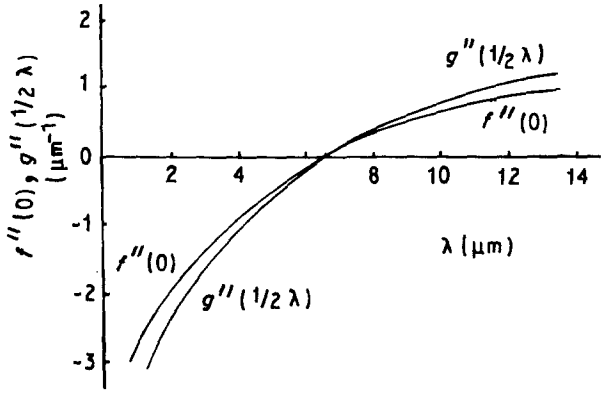

Figure 8 The calculated $f''(0)$ and $g''(\lambda/2)$ as functions of the spacing, λ, for directional solidification of Al–Al_2Cu eutectic. $V = 2.00\ \mu m\ s^{-1}$, $G = 110\ K\ cm^{-1}$.

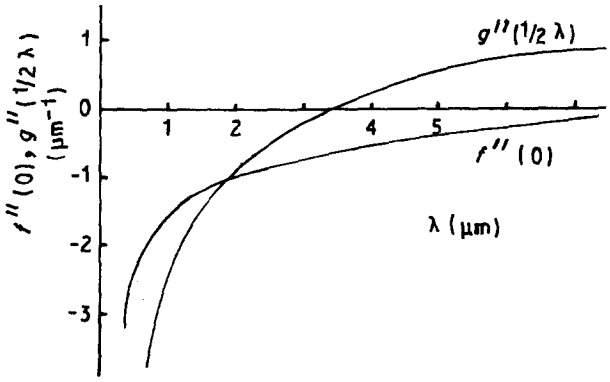

Figure 9 The calculated $f''(0)$ and $g''(\lambda/2)$ as functions of the spacing, λ, for directional solidification of Sn–Pb eutectic. $V = 30.00\ \mu m\ s^{-1}$; $G = 100\ K\ cm^{-1}$.

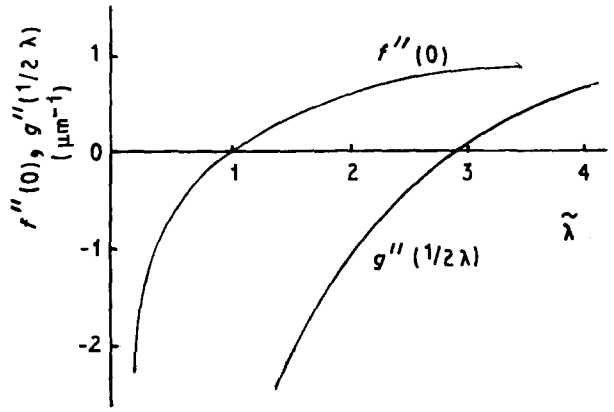

Figure 10 The calculated $f''(0)$ and $g''(\lambda/2)$ as functions of the spacing, λ, for directional solidification of Al–Si eutectic. $V = 10.00\ \mu m\ s^{-1}$, $G = 110\ K\ cm^{-1}$.

(for Al–Si eutectic, ΔT_0^{β}) reaches its minimum value, $\min(\Delta T_0)$, at least, the interfacial profile of one lamellar phase is in the critical splitting state (CSS), and the other lamellar phase has a super-stable solidifying interface. We also found that $f''(x = 0)$ and $g''(x = \lambda/2)$ could be formulated as

$$f''(x = 0) \quad (\text{or } g''(x = \lambda/2)) = A \ln(B\tilde{\lambda}) \qquad (8)$$

where A and B are positive constants. If $f''(x = 0)$ (or $g''(\lambda/2)$) intersects with the $\tilde{\lambda}$ axis at $\tilde{\lambda} = 1.0$, $B = 1.0$. This relation will be useful in the following discussion of pattern stability of the solidifying interface.

3.4. Geometric model – the CSS of the solidifying interface

If we only consider cases where there is at least one lamellar phase having its solidifying interface in the CSS, there are five modes, as shown in Fig. 11. For a eutectic, the corresponding modes are determined by the splitting feature of the interface and the mechanical balance condition at the TPCP. For example, for Al–Al_2Cu eutectic, because $\theta_\alpha \sim \theta_\beta$, the α-liquid and β-liquid interfaces almost simultaneously reach the CSS as $\Delta T_0 = \min(\Delta T_0)$; however, for Sn–Pb eutectic, because $\theta_\beta \ll \theta_\alpha$, the α-liquid interface is super-stable ($f''(x = 0) < 0$) when the β-liquid interface reaches the CSS as $\Delta T_0 = \min(\Delta T_0)$.

For Modes (a), (b) and (c), one lamellar phase has the super-stable interface although the interfacial profile of the other lamellar phase is in the CSS. We can prove that the pattern of this interface in the CSS is marginally stable by dynamics. As $f''(x = 0) = 0$ (or $g''(x = \lambda/2) = 0$), we find that $f(x = 0)$ (or $g(\lambda/2)$) as a function of λ will reach its maximum value. Here, only the case of $f''(x = 0) = 0$ is discussed. For the case of $g''(x = \lambda/2) = 0$, a similar derivation can be given.

In the coordinate system shown in Fig. 1, at the TPCP we have $z \equiv 0$. Hence, ΔT_0 in Equation 3a can be treated as a constant. Because $f''(x = 0) = 0$, we have from Equation 3a

$$\Delta T_0 - Gf(x = 0) = \Sigma \qquad (9)$$

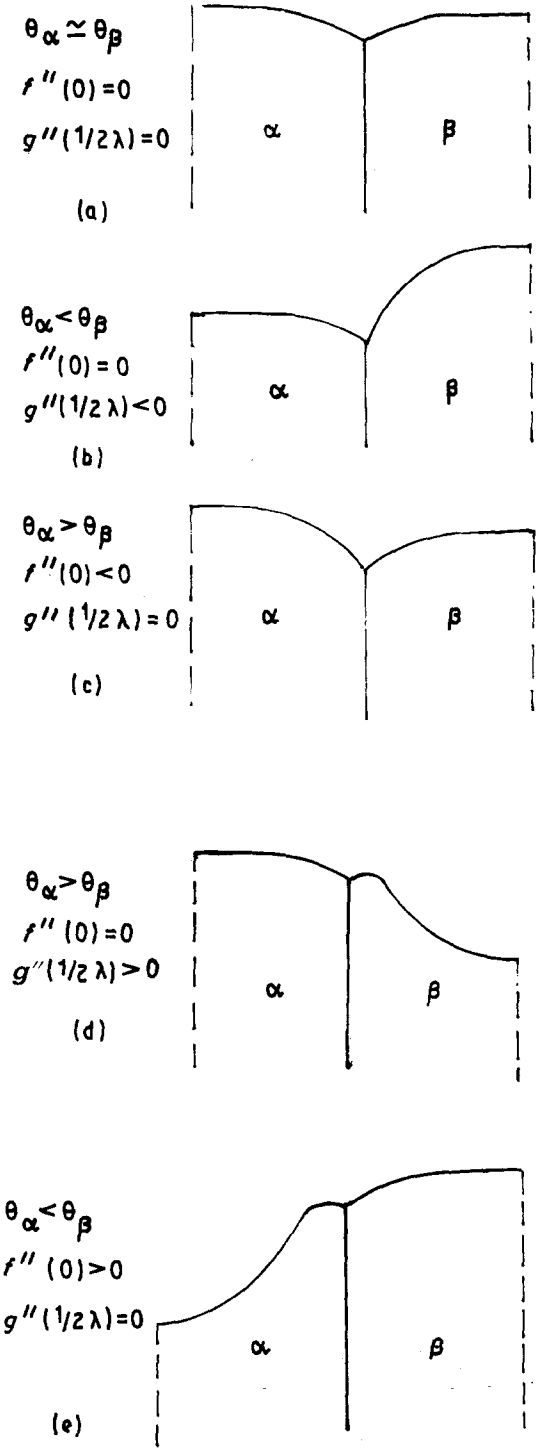

Figure 11 The five modes of spacing selection for directional solidification. (a) CSS α-L and β-L; (b) CSS α-L, β-L; super stable (c) CSS β-L, super-stable α-L; (d) CSS α-L, unstable β-L; (e) CSS β-L, unstable α – L.

where $\Sigma = \sum_{n=1}^{\infty} m_\alpha K$. Let us consider a fluctuation of the spacing, $\Delta\lambda$; as the first-order approximation we have

$$\Delta T_0 - G[f(x = 0) + \Delta f] = \Sigma + \Delta\Sigma - \Gamma^\alpha \Delta f'' \qquad (10)$$

where Δf, $\Delta\Sigma$ and $\Delta f''$ are the corresponding fluctuations of $f(x = 0)$, Σ and f'', respectively. Combin-

ing Equations 9 and 10, we obtain

$$G\Delta f = \Gamma^{\alpha}\Delta f'' - \Delta\Sigma \quad (11)$$

From Equation 3a and c, we have $\Delta\Sigma = a\Delta\lambda$, where a is a positive constant. From Equation 8 we have $\Delta f'' = b(\Delta\lambda/\lambda)$, where b is also a positive constant. Finally we obtain

$$G\Delta f = [\Gamma^{\alpha}(b/\lambda) - a]\,\Delta\lambda \quad (12)$$

As $\Delta\lambda \Rightarrow 0$, Equation 12 becomes

$$G\frac{df(x=0)}{d\lambda} = \Gamma^{\alpha}(b/\lambda) - a \quad (13a)$$

$$Gf(x=0) = \Gamma^{\alpha} b\ln\lambda - a\lambda + C \quad (13b)$$

where C is a constant to be determined. $df(x=0)/d\lambda$ and $f(x=0)$ as functions of λ are drawn schematically in Fig. 12, where $df(x=0)/d\lambda$ is a decreasing function of λ and $f(x=0)$ has a maximum value. For all three eutectics, our calculation shows that when $\lambda = \lambda_1$ (i.e. $f''(x=0) = 0$), $f(x=0)$ reaches its maximum value. This is a meaningful conclusion; physically, the profile of the α-liquid interface always bulges as far as possible into the liquid range when the supercooling ΔT_0 (ΔT_0^{β}) at the TPCP reaches its minimum value. When $\lambda > \lambda_1$, the interface splits, $f(x=0)$ is a decreasing function of λ, as shown in Figs 5–7; when $\lambda < \lambda_1$, $f(x=0)$ becomes an increasing function of λ because of the coupling between thermal transfer and the curvature effect, and restraining of the mechanical balance condition at the TPCP.

From the stability point of view, the solute diffusion in a liquid destabilizes the interface and attracts the interface towards the liquid range ($f(x=0)$ increases), and finally results in midpoint-splitting of the interface. Conversely, the thermal transfer, the curvature effect, and also the mechanical balance condition, restabilize the interface; the former two effects compel the interface to become planar ($|f(x=0)|$ decreases). During the competition between the destabilizing and restabilizing effects, if the former effects are dynamically dominant, the interface profile will bulge as far as possible into the liquid range. Thus, dynamically, the interfacial pattern will approach as much as possible, the stability limit for Modes (a), (b) and (c). This limit is naturally similar to Langer's marginal stability principle of the tip point of needle crystal growth [5, 19]. As Langer has verified, the marginal stability criterion coincides with the minimum supercooling conjecture, assuming a planar interfacial profile [8, 9]. In the above section we have proved that the CSS of the interfacial profile of one lamellar phase (the other lamellar phase having the super-stable interface) corresponds to the minimum value state of supercooling at the TPCP. Therefore, we are convinced that we can now extend Langer's marginal stability theory [8, 9] into a geometrical model: during directional solidification, a lamellar eutectic will have one solidifying interface in the CSS and the other interface will be super-stable.

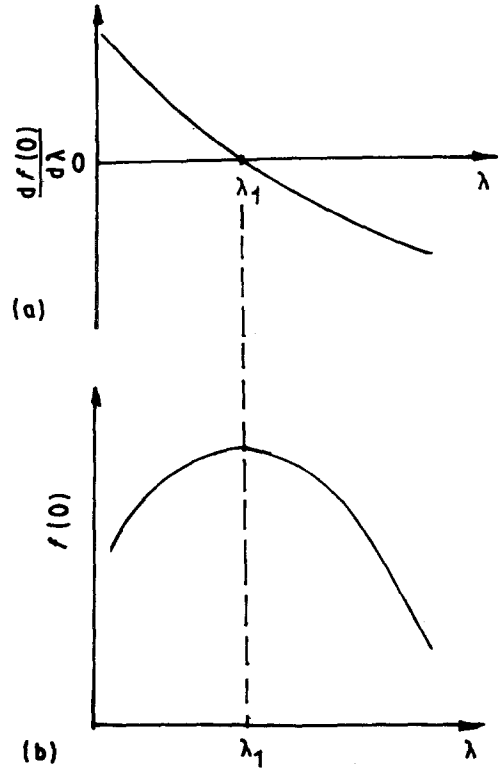

Figure 12 The spacing dependence of (a) $f'_{\lambda}(0)$ and (b) $f'_{\lambda}(0)$ drawn schematically.

It is useful to compare this geometrical model with Langer's marginal stability theory for needle crystal growth [5]. By comparison, it can be clearly shown that the geometrical model is physically reasonable. At first, Langer proved that the steady-state needle crystal selects its tip radius $\rho = \rho^*$, at which the tip point is marginally stable. If $\rho > \rho^*$, the tip of this needle crystal will become unstable, and tip splitting will occur. For the present geometrical model, a critical spacing, λ_1, also exists if $\lambda > \lambda_1$, the interfacial profile of one lamellar phase will become unstable and mid-point splitting will occur for this interface. Secondly, for needle crystal growth, as $\rho = \rho^*$, the position of the tip point reaches the maximum value (in the coordinate system, moving with the growing interface). For eutectic solidification, as $\lambda = \lambda_1$, the midpoint of the interface in the CSS also reaches its maximum value (in the coordinate system shown in Fig. 1).

3.5. Geometrical model of irregular eutectic solidification

In Section 3.3 we investigated the stability of Modes (a), (b) and (c) shown in Fig. 11. In this section. Modes (d) and (e) will be discussed further.

Modes (d) and (e) are obviously unstable because one lamellar phase has a split interfacial profile, although the other lamellar phase has a critical splitting interface. In the liquid range in front of the concave part of the split interface, the constitutional supercooling effect is dominant and the curvature effect is weak. A new lamella easily forms in this liquid range. If a eutectic selects Mode (d) or (e) during directional solidification, the forming lamellar structure is predicted to be irregular. For these eutectic systems with a small value of ratio ε, such as Al–Si eutectic and borneol–succinonitrile eutectic, usually the α lamella

has a splitting solidifying interface. The directionally solidified structures of these eutectics are irregular [20]. *In situ* observation of the solidifying interface of borneol–succinonitrile eutectic [21] supports our discussion of the instability of Modes (d) and (e), and predicts that the formation of irregular structures for these eutectics with low ε follows Mode (d) or (e).

3.6. Scaling law of eutectic solidification

In Sections 3.4 and 3.5, we have proposed two geometrical models. Here, we calculate the scaling relation for directional solidification of the three eutectics, according to the two models. For directional solidification of Al–Al_2Cu eutectic and Sn–Pb eutectic, Modes (a) and (c), respectively, will be followed. We find the spacing λ satisfies the following scaling law

$$\lambda \sim V^{-1/2} f(G/V) \qquad (14)$$

where f is an increasing function of V and saturates at high V. As V is high, this scaling returns to Equation 2. Fig. 13 shows the dependence of f on V, for Al–Al_2Cu eutectic with $G = 100\,\mathrm{K\,cm^{-1}}$ and for Sn–Pb eutectic with $G = 110\,\mathrm{K\,cm^{-1}}$. f can be expressed as an exponential function of V.

For Al–Al_2Cu eutectic

$$f \sim \exp(-0.79\,G/V) \qquad (G \text{ in } K\,\mu m^{-1},\ V \text{ in } \mu m\,s^{-1}) \qquad (15)$$

For Sn–Pb eutectic

$$f \sim \exp(-0.3355\,G/V) \qquad (G \text{ in } K\,\mu m^{-1},\ V \text{ in } \mu m\,s^{-1}) \qquad (16)$$

Obviously the formation of local regular structure of Al–Si eutectic during directional solidification will follow Mode (b); the scaling law differs in form from Equation 14

$$\lambda \sim V^{-1/2} f(G^{1/2}/V) \qquad (17)$$

where f is also an increasing function of V and saturates at high V, which can be expressed as

$$f \sim \exp(-0.0513\,G^{1/2}/V) \qquad (G \text{ in } K\,\mu m^{-1},\ V \text{ in } \mu m\,s^{-1}) \qquad (18)$$

In fact, Equations 15 and 17 are general scaling laws of λ, and take into account the temperature-gradient effect of spacing selection, although this dependence only becomes considerable at low V, as shown in Section 3.2. Kassner and Misbah [15] recently derived a similarity law of eutectic solidification by complex numerical solving of a non-linear integral-differential equation. This law is consistent in form with Equations 14 and 17. This is strong theoretical proof of the validity of our geometrical model. Comparing Equations 14 and 17 with Equation 2, we find that when $V > 10\,\mu m\,s^{-1}$, Equation 2 is a good approach to Equations 14 and 17. Therefore, Equations 14 and 17 are two general scaling laws.

Although Modes (d) and (e) are dynamically unstable, under the steady-state condition we still calculate the scaling law according to these modes. Select solidification of Al–Si eutectic as an instance. The calculated scaling law is

$$\lambda \sim V^{-1/n} h(G) \qquad 2 < n < 3 \qquad (19)$$

where h is a decreasing function of G, which can be expressed as

$$h \sim G^{-0.022} (G \text{ in } K\,\mu m^{-1}) \qquad (20)$$

The validity of Equation 19 is checked below, using our experimental results.

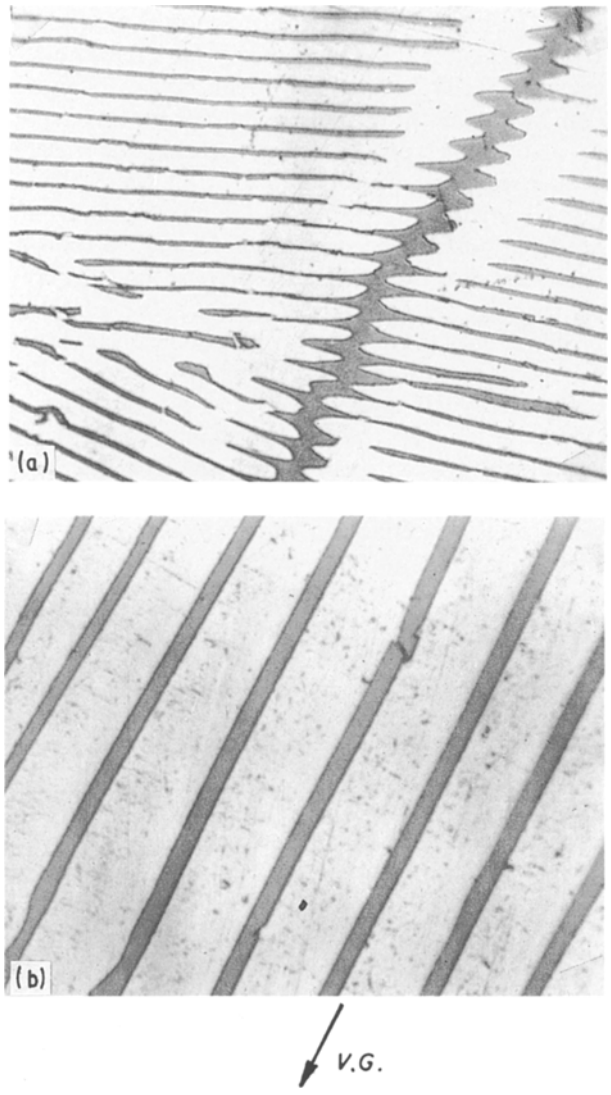

Figure 13 Optimal micrographs of the regular structure Al-Si eutectic forming during directional solidification. (a) $V = 3.10\,\mu m\,s^{-1}$, $G = 149\,K\,cm^{-1}$, radial section. (b) $V = 0.29\,\mu m\,s^{-1}$, $G = 106\,K\,cm^{-1}$, longitudinal section.

4. Experiments and comparison

In recent years some experimental data on directional solidification of the three eutectics have accumulated [2, 3, 22], in which $V \geq 10\,\mu m\,s^{-1}$. As $V \geq 10\,\mu m\,s^{-1}$, the difference between the classic scaling law (Equation 2) and the general scaling laws (Equations 14 and 17), will be hard to distinguish. Naturally, when $V > 10\,\mu m\,s^{-1}$, Equations 14 and 17 are no doubt valid. Further checking of the two laws

requires new experimental data with low V, down to 0.1 $\mu m\,s^{-1}$, as reported by Kassner and Misbah [15]. Here we will restrict our attention to checking the case for Al–Si eutectic, because for this eutectic both local regular lamellar structure and irregular structure form when V is less than 10 $\mu m\,s^{-1}$. This provides the opportunity to check the validity of Equation 17 and 19 at the same time.

The experiments were performed on a unidirectional solidification apparatus, in which steady-state directional solidification with V as low as 0.2 $\mu m\,s^{-1}$ can be obtained. The detailed procedure of the experiment is described elsewhere [20, 22]. Unfortunately, it is not easy to obtain much data for solidification with such a low V, because a large amount of effort is required for each successful experiment.

Fig. 13 shows two typical micrographs of the local regular structure. The spacing of the local regular structure is denoted by λ_r. The measured spacing, λ_r, and the calculated spacing, λ_c, according to Equation 17, are listed in Table II. Good consistency of λ_c with λ_r proves the validity of the scaling law, Equation 17.

TABLE II The measured and calculated spacings of local regular structure of Al–Si eutectic during directional solidification

Sample	V ($\mu m\,s^{-1}$)	G ($K\,cm^{-1}$)	λ_r (μm)	λ_c (μm)
01	0.29	106	14.97 ± 0.48	15.06
02	0.57	149	11.04 ± 0.35	11.18
03	1.03	78	8.01 ± 0.37	8.37
04	1.05	149	7.97 ± 0.39	8.27
05	5.00	149	3.85 ± 0.11	3.81
06	6.62	89	3.10 ± 0.24	3.31
07	10.00	78	2.60 ± 0.15	2.70

For the irregular structure, a typical micrograph of the quenched solid–liquid interface can be found elsewhere [20]. Fig. 14 shows the irregular structure observed along the longitudinal section. The main feature of the middle range of the α-liquid interface is that it is deeply concave into the solid side, as also reflected by the calculated profile of the solidifying interface with large λ, as shown in Fig. 7, although the quenched interface profile is irregular.

In experiments, we have applied the thermal-difference amplifying method to measure the interface supercooling [22], which corresponds to the average of $\overline{\Delta T_\alpha}$ and $\overline{\Delta T_\beta}$. The measured supercooling, ΔT_m, and the calculated supercooling, $\overline{\Delta T_c} = (\overline{\Delta T_\alpha} + \overline{\Delta T_\beta})/2$, are listed in Table III, where λ_m and λ_c are, respectively, the measured average spacing and the calculated spacing according to Equation 19, for the irregular structure of Al–Si eutectic during directional solidification.

From Table III, we are convinced by the excellent agreement of the measured and calculated data that the solidifying interface of irregular structure selects its average spacing according to the Mode (e), although we cannot give precise proof of this dynamical mode from the view point of instability dynamics. So far, to our knowledge, no model can obtain such strong support from experiments, hence there is no reason to prevent us undertaking a further study of this dynamical mode: e.g. the instability analysis, etc. However,

TABLE III Comparison of the theoretical and experimental data for the directional solidification of irregular structure of Al–Si eutectic

Sample	V ($\mu m\,s^{-1}$)	G ($K\,cm^{-1}$)	λ_m (μm)	λ_c (μm)	ΔT_m (K)	ΔT_c (K)
01	0.10	110	56.4[a]	59.00	/	0.11
02	0.63	78	28.03 ± 1.72	29.32	0.25	0.38
03	1.00	110	24.36 ± 2.53[b]	28.00	0.42[b]	0.41
04	5.43	43	13.62 ± 0.92	10.86	1.34	1.04
05	5.10	91	13.33 ± 2.54	11.00	0.96	0.98
06	5.05	101	12.20 ± 2.51	11.25	0.86	0.97
07	5.18	149	9.66 ± 0.90	10.80	0.86	0.88
08	11.36	43	9.54 ± 1.41	7.69	2.14	1.62
09	9.71	63	9.34 ± 2.17	8.21	2.02	1.34
10	10.00	110	7.90 ± 0.70[b]	7.90	1.56[b]	1.34
11	9.95	129	8.41 ± 1.23	7.98	2.17	1.40
12	9.66	149	8.02 ± 0.32	8.07	1.46	1.38
13	20.45	43	8.21 ± 1.92	5.85	2.92	2.05
14	20.12	96	6.60 ± 0.74	5.79	2.74	2.10
15	19.50	106	6.23 ± 0.85	5.86	1.84	2.00
16	20.00	110	6.30 ± 0.60[b]	5.80	1.94[b]	2.01
17	20.50	149	5.61 ± 0.39	5.68	2.26	2.02
18	40.00	101	5.47 ± 0.41	4.19	3.35	2.80
19	39.47	103	5.50 ± 0.44	4.22	3.28	3.15
20	40.00	110	4.20 ± 0.40[b]	4.00	3.11[b]	2.84
21	50.00	110	3.80 ± 0.40[b]	3.58	3.45[b]	3.23
22	70.00	96	4.00 ± 0.59	3.23	3.89	3.90
23	74.90	107	4.03 ± 0.60	3.12	3.56	3.58
24	80.00	110	3.20 ± 0.40[b]	2.95	3.85[b]	3.20
25	100.00	110	2.90 ± 0.30[b]	2.58	4.31[b]	4.51
26	121.00	77	2.76 ± 0.20	2.51	6.11	5.30
27	200.00	110	2.10 ± 0.30[b]	1.98	6.40[b]	6.75

[a] Data derived from the regression equation.
[b] From [23].

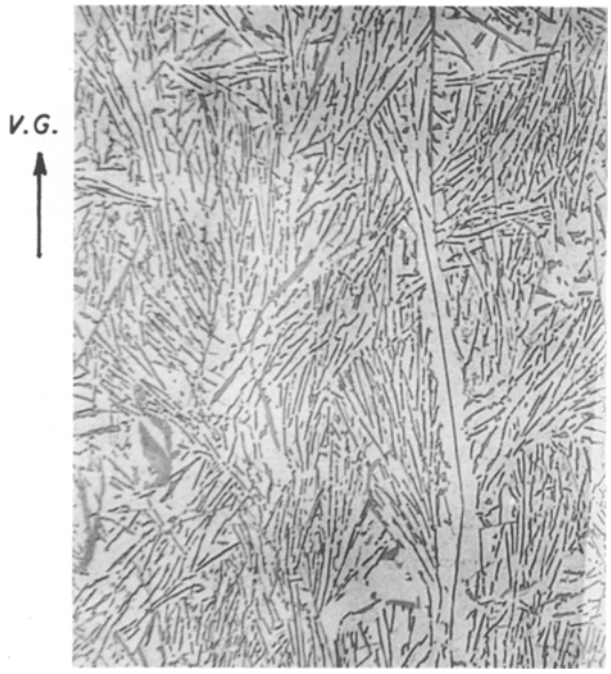

Figure 14 The irregular structure of Al–Si eutectic during directional solidification. $V = 10.0\ \mu m\ s^{-1}$, $G = 89\ K\ cm^{-1}$, longitudinal section.

some problems do exist in our calculation. First, for the case of Al–Si eutectic, we tolerate the abrupt change of supercooling at the TPCP from ΔT_0^{α} to ΔT_0^{β}, which is physically unreasonable. Secondly, we have given no precise mathematical proof of the two geometrical models. Finally, we have not applied the two models to other solidification systems and thus we do not know whether or not they are general. These problems will be the aims of a further study.

5. Conclusion

In conclusion, we have solved numerically the nonlinear steady-state coupling equation of directional solidification of Al–Al_2Cu, Sn–Pb and Al–Si eutectics. The supercooling at the TPCP, the average supercooling, the profiles and the splitting features of the solidifying interface have been studied in detail as functions of the lamellar spacing under different growth rates and temperature gradients.

We have found that when the spacing increases, the profile of the solidifying interface evolves from a state bulging into the liquid range, to a state with the middle parts being considerably concave in the solid side. A critical value of the spacing exists at which at least one lamellar phase has the critical splitting solidifying interface, and the solidifying interface of the other lamellar phase bulges into the liquid range (i.e. it is super-stable). As a function of the spacing, the supercooling at the TPCP reaches its minimum value at this critical spacing. We have proved that at this critical spacing, the critical splitting interface is marginally stable. We therefore have proposed a geometrical model followed by the spacing selection, from which the new general scaling laws for the three eutectics are derived. These laws coincide in form with the similarity law recently derived by Kassner and Misbah [15].

We have also proposed another geometrical model followed by the formation of irregular structure for the eutectics with low volume ratio of the two lamellar phases. For the case of Al–Si eutectic, a new scaling law is derived according to this model.

The precise experimental results of directional solidification of Al–Si eutectic have been presented. The measured data of the spacing of local regular structure and the average spacing of the irregular structure are consistent with our calculated results. The present experimental results for directional solidification of the three eutectics support our two geometrical models.

References

1. H. J. SPRENGER, J. POTSCHKE, C. POTARD and V. ROGGE, in "Fluid Sciences and Materials Science in Space", edited by H. U. Walter (Springer, Berlin, (1987) p. 569.
2. R. ELLIOTT, "Eutectic Solidification Processings" (Butterworths, London, 1983).
3. H. MULLER-KRUMBHAAR and W. KURZ, in "Materials Science and Technology: A Comprehensive Treatment", edited by R. W. Cahn, P. Hassen and E. J. Kramer (VCH, New York, 1991) p. 554.
4. K. A. JACKSON and J. D. HUNT, *Trans. Metall. AIME* **236** (1966) 1129.
5. J. S. LANGER, *Rev. Mod. Phys.* **52** (1980) 1.
6. D. BENSIMON, L. P. KADANOFF, S. LIANG, B. SHARIMAN and C. TANG, *ibid.* **58** (1986) 997.
7. C. ZENER, *Trans. Metall. AIME* **167** (1974) 550.
8. J. S. LANGER, *Phys. Rev. Lett.* **44** (1980) 1023.
9. V. DAYTE and J. S. LANGER, *Phys. Rev. B* **24** (1981) 4155.
10. H. E. CLINE, *J. Appl. Phys.* **50** (1979) 4780.
11. *Idem, ibid.* **52** (1981) 256.
12. *Idem, ibid.* **53** (1982) 4896.
13. *Idem, Mater. Sci. Engng* **65** (1984) 93.
14. *Idem, Metall. Trans.* 15A (1984) 1013.
15. K. KASSNER and C. MISBAH, *Phys. Rev. Lett.* **66** (1991) 445.
16. J.-M. LIU, Y.-H. ZHOU and B.-L. SHANG, *Acta Metall.* **38** (1990) 1625.
17. W. KURZ and D. J. FISHER, "Fundamentals of Solidification' (Trans. Tech, Aedermannsdorf, 1984).
18. M. GUNDUZ and J. D. HUNT, *Acta. Metall.* **33** (1985) 1651.
19. D. KESSLER, J. KOPLIK and H. LEVINE, *Adv. Phys.* **37** (1988) 255.
20. J.-M. LIU, Y.-H. ZHOU and B.-L. SHANG, *Acta. Metall.* **38** (1990) 1631.
21. D. J. FISHER and W. KURZ, *ibid.* **28** (1980) 777.
22. J.-M. LIU, Y.-H. ZHOU and B.-L. SHANG, *J. Mater. Sci.* **27** (1992) 2067.
23. L. M. HOGAN and H. SONG, *Metall. Trans.* **18A** (1987) 707.

Received 22 January
and accepted 20 November 1992